BJR

https://doi.org/10.1259/bjr.20170569

Received: 05 August 2017 | Revised: 18 April 2018 | Accepted: 22 April 2018

Cite this article as:
Sun K, Han R, Zhao R, Bai S, Wang J, Hu J, et al. Evaluation of dual energy computed tomography iodine mapping within the myocardial blood pool for detection of acute myocardial infarction: correlation with histopathological findings in a porcine model. *Br J Radiol* 2018; **91**: 20170569.

FULL PAPER

Evaluation of dual energy computed tomography iodine mapping within the myocardial blood pool for detection of acute myocardial infarction: correlation with histopathological findings in a porcine model

[1,2]KAI SUN, [3]RUIJUAN HAN, [3]RUIPING ZHAO, [2]SHUANCHENG BAI, [2]JUNYAN WANG, [3]JIANG HU and [1]BIN LU

[1]Department of Radiology, State Key Laboratory of Cardiovascular Disease, Fu Wai Hospital, National Center for Cardiovascular Diseases, Chinese Academy of Medical Sciences and Peking Union Medical College, Beijing, China
[2]Department of Radiology, Baotou Central Hospital, Inner Mongolia, Baotou, China
[3]Translational Medicine Research Center, Baotou Central Hospital, Inner Mongolia, Baotou, China

Address correspondence to:
Dr Bin Lu
E-mail: *bin_lu1@163.com*
Jiang Hu
E-mail: *Jianghu1961@163.com*

The authors Kai Sun and Ruijuan Han contributed equally to the work.

Objective: We assessed the diagnostic value of "one-step" dual energy CT (DECT) in combination with coronary CT angiography and iodine mapping within the myocardial blood pool in detecting acute myocardial infarction (AMI).

Methods: Five minipigs were subjected to transcatheter embolization of coronary artery with a gelatin sponge to induce AMI. Arterial-phase myocardial DECT imaging was carried out 1 h before and 24 h after embolism of the coronary. Color-coded iodine maps were used to evaluate myocardial blood pool deficits in the 17-segment model. Myocardial DECT imaging 24 h after MI induction was used for final comparison with post-mortem histology.

Results: We found a sensitivity of 95.55% and a specificity of 95%, respectively, for AMI detection by DECT-based iodine mapping within the myocardial blood pool. The dose–length product values were 219.4 ± 60.9 mGy.cm (172–321 mGy.cm) and the effective radiation dose was 5.7 ± 1.5 mSv (4.4–8.3 mSv).

Conclusion: This experimental study demonstrated that DECT-based iodine mapping shows a high value for the detection of myocardial perfusion defects in the first-pass myocardial perfusion. Hybrid heart images obtained by coronary CT angiography and DECT-based iodine mapping may yield valuable data and help clinicians accurately identify cases requiring further treatment after AMI.

Advances in knowledge: This study demonstrated that DECT-based iodine mapping is a promising new technique for the detection of myocardial perfusion defects in the first-pass myocardial perfusion.

INTRODUCTORY SECTION

Heart CT, a non-invasive technique, is highly accurate in diagnosing coronary arterial stenosis.[1] However, it does not clearly define the hemodynamic significance of lesions. Despite the efficacy of single photon emission CT and positron emission tomography for the quantitative analysis of myocardial blood flow and coronary flow reserve, these techniques do not allow the evaluation of coronary stenosis due to poor spatial resolution.[1] Extensive data related to the prognostic value of myocardial perfusion imaging suggest infarct and ischemic burden correlate with long-term outcomes in distinguishing the patients most appropriate for revascularization from those indicated for medical therapy. Therefore, combining anatomical findings derived from CT angiography with physiological data from perfusion may enhance the diagnostic value.[2] Dual energy CT (DECT) makes it possible to simultaneously use two different tube voltages, allowing different X-ray absorption features to be obtained at the same anatomic site with two distinct X-ray spectra.[3,4] Preliminary experimental and human studies suggest DECT provides a one-step imaging for determining coronary morphology and myocardial

blood supply, with findings highly corroborating those derived from invasive coronary angiography, single photon emission CT and MRI.[5–7] Although initial reports have applied first-pass dual energy perfusion CT for detecting myocardial perfusion anomalies,[8] few studies have evaluated the accuracy of dual energy iodine mapping in diagnosing acute myocardial infarction (AMI), including histopathological findings as reference. The present work assessed the diagnostic value of DECT combined with coronary CT angiography and iodine mapping—blood distribution—within the myocardium for detecting AMI using second generation dual source CT in comparison with histopathological data, in pigs.

METHODS AND MATERIALS

Ethical statement

The present study had approval from the Capital Medical University Animal Care and Use Committee, and was carried out following the Guide for the Care and Use of Laboratory Animals recommended by the Association for Assessment and Accreditation of Laboratory Animal Care International.

Animal model

A total of five pigs (Taihe Biotechnology Co., Taizhou, China; 25–34 kg) were used. Exams were carried out under general anesthesia and monitored continuously by electrocardiography. The pigs were anesthetized by intramuscular injection of 6 mg kg^{-1} ketamine (Fujian Gutian Pharmaceutical Co., China), midazolam (0.2 mg kg^{-1}; Jiangsu Enhua Pharmaceutical Group Co., China) and penehyclidine hydrochloride (1 mg; Chengdu Lisi Pharmaceutical Co., Ltd., China). In addition, the animals received propofol at 3.5 mg kg^{-1}. Anesthesia maintenance was performed by continuously providing 6–8 mg kg^{-1} h^{-1} propofol intravenously. Such protocol was employed for myocardial infarction (MI) induction and final CT exams. In dual energy CT, esmolol hydrochloride (0.15–0.3 mg kg^{-1}·min; Qilu Pharmaceutical Co., Ltd., Shandong, China) was injected continuously to reduce the heart rate (targeting a heart rate of <100 beats min^{-1}) .

MI induction

The MI induction process was guided by selective coronary angiography with gelatin sponge as an embolic agent. A 6-Fr introducer sheath was introduced in a femoral artery, followed by administration of 10,000 IU heparin (Changzhou Pharmaceutical Co., China). Subsequently, 1000 IU heparin was administered on an hourly basis. A 5-Fr guiding catheter (Medtronic, USA) was introduced in the left or right coronary artery (RCA) via the introducer sheath. This was followed by the placement of the guide wire between the first and second diagonal branches of the left anterior descending (LAD) or at the midpoint of the RCA. Then, a 3-Fr balloon (2.0 × 20 mm, Medtronic Co., USA) was positioned at the distal end of the second LAD diagonal or midpoint of the RCA. To protect from ischemic injury and reduce mortality, the balloon was dilated about 180 s for ischemic preconditioning,[9] blocking blood flow for 1, 2 and 5 min, respectively, at 60 s intervals. Next, gelatin sponge (1.5 × 1.5 mm) injection into the midpoint of the LAD (two pigs) or distal end of the RCA (one pig). Two additional pigs had occlusions of both the LAD (as described above) and proximal circumflex artery. Ventricular fibrillation during balloon occlusion was immediately followed by defibrillation. The pigs were fed a high protein diet for 24 h, with water for rehydration, to compensate for blood loss during MI induction.

Scan protocols and image reconstruction

The retrospective electrocardiographic-gated dual energy mode on a second-generation 128-slice DSCT (Definition Flash, Siemens Healthcare, Forchheim, Germany) was used for all scans. Arterial-phase myocardial DECT was carried out 1 h before and 24 h after embolism to evaluate the absence of myocardial blood flow. The dual energy CT mode was characterized by 280 ms gantry rotation, pitch of 0.17 for spiral modes, collimation 2 × 64 × 0.6 mm/2 × 128×0.6 mm with a z-flying focal spot, and 150 mAs per rot tube current at Sn140 kVp to 165 mAs per rot at 100 kVp. The contrast agent iohexol (350 mg ml^{-1}; GE Healthcare, USA) was provided intravenously at 1.5 ml kg^{-1} and 4 ml s^{-1}. Flushing was carried out with 40 ml saline administered once. Data acquisition started after reaching the threshold in the ascending aorta (mean delay of 4 s).

By default, raw data were automatically reconstructed into three separate image sets: low-kilovoltage (100 kV), high-kilovoltage (140 kV), and linearly blended image sets. The linearly blended images used a weighting factor of 0.3, combining 30% of 100 kV data and 70% of 140 kV data. Then, the linearly blended images were used at 1.0 mm slice thickness and 0.75 mm intervals with a D30 dual energy cardiac kernel, and subsequently processed on a commercially available workstation (Syngo MMWP, VA36, Siemens Healthcare) with an associated software to generate myocardial "iodine maps" in the short and long axes (four views). The iodine maps representing the myocardial blood pool were 16-bit color-coded and overlayed with grayscale anatomic multiplanar reformatted myocardial images to form "iodine maps". The latter were further overlayed with grayscale multiplanar reformatted virtual non-enhanced myocardial images in short- and long-axis views of the left ventricle. Color coding was carried out using shades of green, with bright green and black representing high and no iodine, respectively. To evaluate the coronary artery, CT angiography images were reconstructed with retrospective electrocardiographic-gating and single-segment reconstruction in best diastolic (heart rate ≤70 bpm) or systolic (heart rate >70 bpm) phase (BestPhase, Siemens Healthcare, Germany): slice thickness, 0.75 mm and 0.4 mm increment; medium-soft convolution kernel (B26f). Curved planar reformatting (thickness 8.0 mm), maximum intensity projection (thickness 10.0 mm), multiplanar reformatting and volume rendering were employed for coronary artery assessment.

Image interpretation

Two radiologists (3 and 5 years of experience, respectively, in cardiac imaging) with no knowledge of histopathological data and reconstruction procedure evaluated the three DECT series obtained after reconstruction, in an independent and random manner. Sensitivity, specificity, and positive- (PPVs) and negative-predictive values (NPVs) for MI detection were derived for all imaging modalities, respectively, following

Figure 1. Standard classification of segmental myocardial regions for CT myocardial perfusion imaging. LAD, left anterior descending; LCx, left circumflex artery; RCA, right coronary artery.

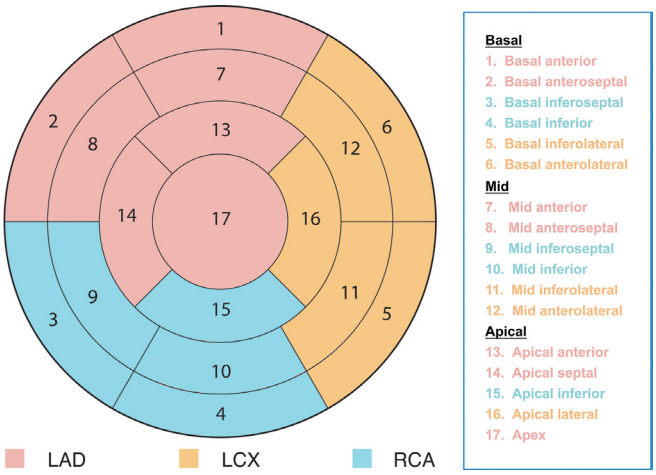

the standard classification of myocardial 17-segment model (Figure 1), compared with histopathological data.

Estimation of radiation dose

The volume CT dose index and dose–length product (DLP) were recorded after single scans. Effective radiation doses (mSv) were derived as DLP values multiplied by a cardiac-specific coefficient of 0.026 $mSv \cdot mGy^{-1} \cdot cm^{-1}$, according to the latest report by JACC: Cardiovascular Imaging.[10]

Histopathological assessment

Histopathological findings were considered the diagnostic reference. Myocardial DECT imaging 24 h after MI induction was used for final comparison with post-mortem histology. After the final CT scan, which was performed 24 h after MI induction, all the animals were euthanized. This was followed by heart excision and storage at −20°C for 60 min. Along the short axis, the left ventricle was cut into 3-mm-thick sections, treated with 1% triphenyl-tetrazolium chloride (TTC), and submitted to staining (37°C and 1 h) for histopathology. Infarction cases were verified by hematoxylin and eosin (H&E) staining and electron microscopy for all 17 left ventricular segments, respectively.

Statistical analysis

Statistical analyses were carried out with SPSS19.0 (SPSS, USA). Measurement data are mean ± standard deviation. With pathological data as diagnostic reference, sensitivity, specificity, and PPVs and NPVs of DECT-based iodine mapping for detecting myocardial ischemia were assessed. Between-observer consistency was determined by the Cohen's κ method.

RESULTS

MI modeling was successful in all pigs, with one having a distal occlusion of the RCA and two showing occlusions both in the middle segment of LAD and proximal circumflex artery (Although LAD was the target coronary, gelatin sponge embolus refluxed into proximal circumflex artery and the proximal circumflex artery was obstructed by gelatin sponge embolus in two pigs, which were obstructed both in LAD and the proximal circumflex artery.) . Meanwhile, two animals had a single occlusion in the middle segment of LAD. A total of two animals manifested ventricular tachycardia during LAD occlusion and were successfully treated with lidocaine administered intravenously. Animal weights were 29 ± 3.8 kg, ranging from 25 to 34 kg; heart rates were 102 ± 18 bpm, ranging between 80 and 128 bpm.

Figure 2. H&E staining depicting infarcted myocardial lesions (arrow) and normal intersperse myocardial foci, detectable at low magnification by microscopy (a). At high magnification, myocardial cytoplasm cohesion, eosinophil level alteration, stripe disappearance, nucleus relocation, and interstitial edema of cardiomyocytes were detected (arrow) (b). H&E, hematoxylin and eosin.

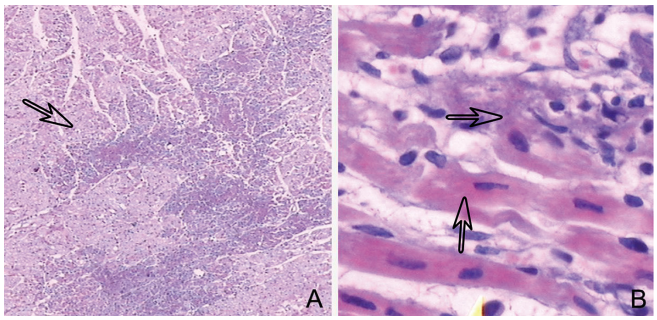

Histopathology findings

The normal myocardium stains red, but appears white after treatment with triphenyl-tetrazolium chloride. Histopathological findings revealed 46 segmental myocardial regions with MI and 39 normal ones. H&E staining showed myocardial infarcts interspersed with normal myocardial foci, which were visible microscopically at low magnification. Pathological alterations, including myocardial cytoplasm cohesion, eosinophil level variations, stripe disappearance, nuclear relocation, and cardiomyocyte interstitial edema, were visualized at high-magnification by microscopy. A few severely damaged myocardial cells showed no nuclei and basophilic granules. Micrographs of H&E staining of lesions in the infarcted myocardium are shown in Figure 2.

Accuracy of DECT-based iodine mapping using histopathological findings as a reference

In 5 pigs, 85 segmental myocardial regions were evaluated by DECT-based iodine mapping. Using histopathological findings as a diagnostic reference, DECT-based myocardial iodine mapping correctly diagnosed 43 of the 46 infarcted segmental myocardial regions, and 37 of the 39 non-infarcted segmental myocardial regions for Reader 1; 43 of the 46 infarcted segmental myocardial regions and 35 of the 39 non-infarcted segmental myocardial regions were corrected detected by Reader 2. These findings indicated sensitivity of 93.47% and specificities of 94.87 and 89.74% for readers 1 and 2, respectively. A good interobserver agreement for the assessment of iodine distribution in the myocardium was obtained (κ = 0.74). Overall, DECT-based myocardial iodine mapping had 95.55% sensitivity and 95% specificity in comparison with histopathological findings

Table 1. Segmental region and number of myocardial infarction detected by DECT and histopathology

Methods	Myocardial segments																Total
	1	2	3	4	5	6	7	8	9	10	11	12	13	14	15	16	17	
DECT iodine																		
Reader 1	2	2	1	2	2	0	4	4	4	1	4	0	4	4	4	3	4	45
Reader 2	2	2	1	2	3	0	4	5	4	1	4	0	4	4	4	3	4	47
Histopathology	2	2	1	2	2	2	4	4	4	1	4	0	2	4	4	4	4	46

DECT, dual energy CT.

Table 2. Accuracy assessment for DECT Iodine map detection of myocardial infarction

Diagnostic accuracy	Reader 1 (n = 85)	Reader 2 (n = 85)	Overall
True-positive	43	44	43
False-positive	2	4	2
True-negative	37	35	38
False-negative	3	2	2
Sensitivity (%)	93.47	93.47	95.55
Specificity (%)	94.87	89.74	95
Positive-predictive value (%)	95.55	91.48	95.55
Negative-predictive value (%)	92.50	92.11	95

DECT, dual energy CT.

for detection of myocardial perfusion defects. Table 1 displays comparative data of DECT-based iodine mapping and histopathological diagnosis of MI for regions and numbers of ischemic segmental myocardial regions. Parameters reflecting the diagnostic value of DECT-based iodine mapping are indicated in Table 2, including sensitivity, specificity, and predictive values. Data obtained by coronary CT angiography, invasive angiography, and dual energy iodine mapping before MI induction are shown in Figure 3. Representative results of dual energy iodine mapping within the myocardial blood pool for detecting AMI in comparison with pathological findings are illustrated in Figure 4.

Radiation dose

The DLP values were 219.4 ± 60.9 mGy.cm (172–321 mGy.cm). The effective radiation dose was 5.7 ± 1.5 mSv (4.4 –8.3 mSv).

DISCUSSION

This study revealed sensitivity of 95.55% and specificity of 95%, respectively, for AMI detection by DECT-based iodine mapping within the myocardial blood pool. DECT-based iodine mapping shows a high value for the detection of myocardial perfusion defects in the first-pass myocardial perfusion.

Differentiating viable from infarcted myocardium is critical in predicting the improvement of left ventricular function, detecting occult infarcts and identifying cardiovascular risk. Coronary occlusion caused infarction of the ventricular wall in surviving animals as verified by ultrastructural and histological findings. MI is associated with an increased local distribution of contrast agents. Accordingly, scar infarction is observed as hyperenhancement with delayed enhancement CT or MRI. Fenoglio et al[11] used isolated superfused preparations of the infarcted myocardium to assess the cellular electrical activity of subendocardial Purkinje fibers and the ventricular muscle in the first 24 h after occlusion of left anterior descending coronary artery. They found that the number of ventricular muscle cell layers decrease with time after coronary occlusion. At 24 h after occlusion, there were no ventricular muscle cell layers. According to Fenoglio et al,

Figure 3. Coronary CT angiography showing no occlusion in segments of the coronary artery before MI induction (a). Dual energy iodine mapping showing normal blood pool in the middle segmental region of the myocardium before MI induction (b). Invasive angiography (c) confirming obstruction in the middle of left anterior descending artery (red arrow) and left circumflex artery (green arrow). Coronary CT angiography demonstrating the obstruction (d). MI, myocardial infarction.

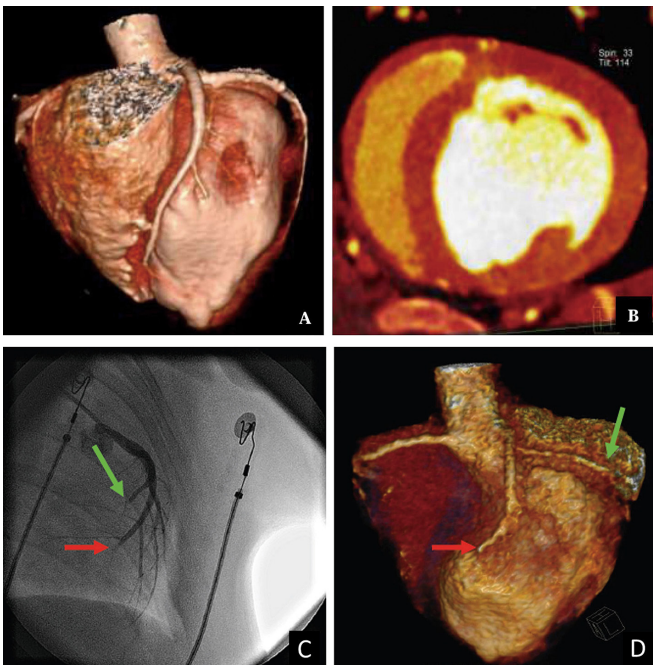

we hypothesized that myocardial iinfarction should be detected at the time point of 24 h after coronary occlusion. Zhang et al[7] performed single contrast-enhanced DECT at 1 day before and 3 h after ligation of the mid segment of the LAD. In this experimental study, the porcine model had a high survival rate because MI induction was guided by selective coronary angiography with gelatin sponge as an embolic agent. Meanwhile, we selected 24 h after coronary occlusion as the optimum time point to evaluate the myocardial perfusion defects in the first-pass myocardial perfusion.

Previous reports assessing the accuracy of DECT-based iodine mapping in detecting myocardial ischemia showed that sensitivity varies from 72 to 93.8%, and specificity between 72 and 99.1%.[7,12–14] As shown above, sensitivity and specificity were 93.47 and 94.87%, respectively, for detecting AMI by DECT-based iodine mapping. In this study, DECT revealed two segmental myocardial regions with false-positive infarcts and two with false-negative results. The false positive findings obtained by DECT-based iodine mapping were attributed to the hibernating myocardium presenting as blood pool deficient segmental myocardial regions in iodine imaging. Indeed, the hibernating myocardium displays low contractility because of decreased perfusion caused by severe coronary artery stenosis. Deseive et al[15] reported that the infarcted myocardium displays higher iodine levels compared with normal myocardial tissues

Figure 4. Representative results of dual energy iodine mapping within the myocardial blood pool for detecting acute myocardial infarction based on pathological findings. Basal segment (a, b), middle segment (c, d), apical segment (e, f), and segments of the apex (g, h). Dual energy iodine imaging (a, c, e, and g) showing blood pool deficit in the myocardial segments 1, 2, 4, 5, 7, 8, 10, 11, 13, and 17 (*) and corresponding myocardial infarction segmental regions (*) in TTC pathology (b, d, f, and h). Myocardial segmental regions 3, 6, 9, 10, 12, 14, and 16 in dual-energy iodine imaging showed normal blood pool and corresponding normal myocardial infarction segmental regions in pathology. Dual-energy iodine imaging (e) showing blood pool deficit (*) in the myocardial segmental region 15, confirmed normal myocardial segmental region (Δ) in TTC pathology (f) (false-positive). TTC, triphenyltetrazolium chloride.

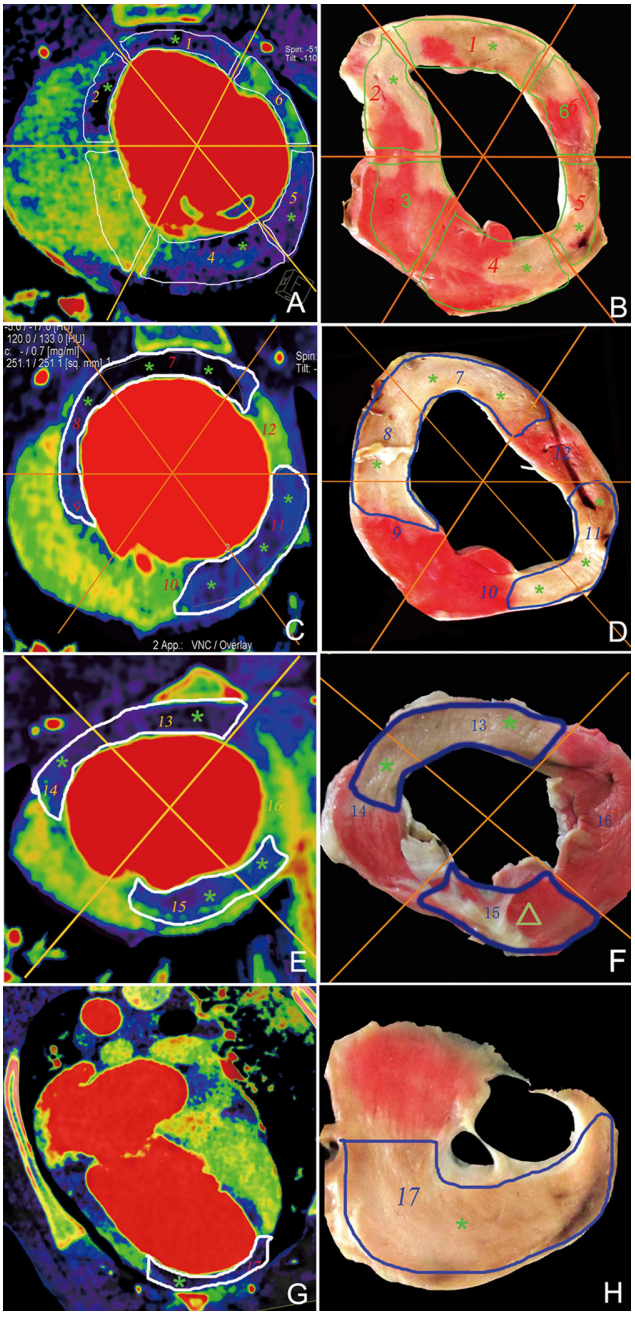

during late enhancement. This study solely focused on AMI detection in single-phase scans rather than delayed enhancement, which may be more sensitive compared with single arterial phase. Beam hardening and heart movement artefacts lead to false-positive findings. False-negative findings were characterized by widely variable myocardial iodine levels, which might be due to iodine level normalization to regions with normal myocardial perfusion.

Radiation doses required by the various CT methods were assessed; radiation doses in the current model were 5.7 ± 1.5 mSv, based on a cardiac-specific coefficient of 0.026 $mSv \cdot mGy^{-1} \cdot cm^{-1}$ proposed by the latest report by *JACC: Cardiovascular Imaging*.

The limitations of the current study should be mentioned. First, the relatively small sample size resulted in reduced statistical power. Therefore, experiments assessing more animals are required to confirm these findings. Secondly, DECT data focused on detecting myocardial perfusion defects early after MI in single-phase scans. Additional investigations combining DECT-based iodine mapping during the arterial phase and delayed enhancement are required to increase diagnostic sensitivity. Future studies may also combine imaging data in the arterial phase and DECT-based delayed enhancement imaging assessment of myocardial viability. DECT may be of particular significance for the latter application; indeed, DECT-based iodine mapping with delayed enhancement may detect subtle regions with higher sensitivity than routine single-source CT. Thirdly, even after administering drugs intravenously to lower the heart rate, a mean value of 102 bpm was obtained, which is higher than that of clinical cases and results in decreased image quality in coronary CT angiography and DECT-based iodine mapping. Fourthly, the sizes of coronary vessels were not assessed, and the sizes of myocardial infarcts revealed by DECT with those observed in histopathology could not be compared because current heart DECT software cannot provide the quantitative measurements of the sizes of myocardial infarcts. Nevertheless, since it would be unethical to obtain histopathological correlations in most clinical studies, animal models are critical to validate the accuracy of CT techniques.

CONCLUSION

This experimental study demonstrated that DECT-based iodine mapping shows high sensitivity and specificity for the detection of myocardial perfusion defects in the first-pass myocardial perfusion. Hybrid heart images obtained by coronary CT angiography and DECT-based iodine mapping may yield valuable data and help clinicians accurately identify cases requiring further treatment after AMI.

FUNDING

This study was supported by research grants from the National Natural Science Foundation of China (81560286), National Key Project of the 13th Five-Year Plan of China (2016YFC1300400) and National Natural Science Foundation of Inner Mongolia Autonomous Region of China (2017MS0853).

REFERENCES

1. Carrascosa P, Capuñay C, Deviggiano A, Goldsmit A, Tajer C, Bettinotti M, et al. Accuracy of low-dose prospectively gated axial coronary CT angiography for the assessment of coronary artery stenosis in patients with stable heart rate. *J Cardiovasc Comput Tomogr* 2010; **4**: 197–205. doi: https://doi.org/10.1016/j.jcct.2010.04.001
2. Kim SM, Choi JH, Chang SA, Choe YH. Detection of ischaemic myocardial lesions with coronary CT angiography and adenosine-stress dynamic perfusion imaging using a 128-slice dual-source CT: diagnostic performance in comparison with cardiac MRI. *Br J Radiol* 2013; **86**: 20130481. doi: https://doi.org/10.1259/bjr.20130481
3. Johnson TR, Krauss B, Sedlmair M, Grasruck M, Bruder H, Morhard D, et al. Material differentiation by dual energy CT: initial experience. *Eur Radiol* 2007; **17**: 1510–7. doi: https://doi.org/10.1007/s00330-006-0517-6
4. Jin KN, De Cecco CN, Caruso D, Tesche C, Spandorfer A, Varga-Szemes A, et al. Myocardial perfusion imaging with dual energy CT. *Eur J Radiol* 2016; **85**: 1914–21. doi: https://doi.org/10.1016/j.ejrad.2016.06.023
5. Ruzsics B, Lee H, Zwerner PL, Gebregziabher M, Costello P, Schoepf UJ. Dual-energy CT of the heart for diagnosing coronary artery stenosis and myocardial ischemia-initial experience. *Eur Radiol* 2008; **18**: 2414–24. doi: https://doi.org/10.1007/s00330-008-1022-x
6. Ruzsics B, Schwarz F, Schoepf UJ, Lee YS, Bastarrika G, Chiaramida SA, et al. Comparison of dual-energy computed tomography of the heart with single photon emission computed tomography for assessment of coronary artery stenosis and of the myocardial blood supply. *Am J Cardiol* 2009; **104**: 318–26. doi: https://doi.org/10.1016/j.amjcard.2009.03.051
7. Zhang LJ, Peng J, Wu SY, Yeh BM, Zhou CS, Lu GM, SY W, GM L. Dual source dual-energy computed tomography of acute myocardial infarction: correlation with histopathologic findings in a canine model. *Invest Radiol* 2010; **45**: 290–7. doi: https://doi.org/10.1097/RLI.0b013e3181dfda60
8. Han R, Sun K, Lu B, Zhao R, Li K, Yang X, et al. Diagnostic accuracy of coronary CT angiography combined with dual-energy myocardial perfusion imaging for detection of myocardial infarction. *Exp Ther Med* 2017; **14**: 207–13. doi: https://doi.org/10.3892/etm.2017.4485
9. Faircloth ME, Redwood SR, Marber MS. Ischaemic preconditioning and myocardial adaptation to serial intracoronary balloon inflation: cut from the same cloth? *Heart* 2004; **90**: 358–60. doi: https://doi.org/10.1136/hrt.2003.025791
10. Trattner S, Halliburton S, Thompson CM, Xu Y, Chelliah A, Jambawalikar SR, et al. Cardiac-specific conversion factors to estimate radiation effective dose from dose-length product in computed tomography. *JACC Cardiovasc Imaging* 2018; **11**: 64-74. doi: https://doi.org/10.1016/j.jcmg.2017.06.006
11. Fenoglio JJ, Karagueuzian HS, Friedman PL, Albala A, Wit AL. Time course of infarct growth toward the endocardium after coronary occlusion. *Am J Physiol* 1979; **236**:

H356–H370. doi: https://doi.org/10.1152/ajpheart.1979.236.2.H356

12. Ko SM, Choi JW, Song MG, Shin JK, Chee HK, Chung HW, et al. Myocardial perfusion imaging using adenosine-induced stress dual-energy computed tomography of the heart: comparison with cardiac magnetic resonance imaging and conventional coronary angiography. *Eur Radiol* 2011; **21**: 26–35. doi: https://doi.org/10.1007/s00330-010-1897-1
13. Nakahara T, Toyama T, Jinzaki M. Quantitative analysis of Iodine Image of dual-energy computed tomography at rest: comparison with 99mTc-tetrofosmin stress-rest single-photon emission computed tomography myocardial perfusion Imaging as the reference standard. *J Thorac Imaging* 2017; **33**: 97–104.
14. Chung HW, Ko SM, Hwang HK, So Y, Yi JG, Lee EJ, et al. Diagnostic performance of coronary CT angiography, stress dual-energy CT perfusion, and stress perfusion single-photon emission computed tomography for coronary artery disease: comparison with combined invasive coronary angiography and stress perfusion cardiac MRI. *Korean J Radiol* 2017; **18**: 476–86. doi: https://doi.org/10.3348/kjr.2017.18.3.476
15. Deseive S, Bauer RW, Lehmann R, Kettner M, Kaiser C, Korkusuz H, et al. Dual-energy computed tomography for the detection of late enhancement in reperfused chronic infarction: a comparison to magnetic resonance imaging and histopathology in a porcine model. *Invest Radiol* 2011; **46**: 450–6. doi: https://doi.org/10.1097/RLI.0b013e3182145b4f